J|A|C|S ARTICLES

Published on Web 06/22/2010

Pressure-Induced Spin-State Transition in $BiCoO_3$

Kengo Oka,*,† Masaki Azuma,*,† Wei-tin Chen,†,‡ Hitoshi Yusa,§ Alexei A. Belik,|| Eiji Takayama-Muromachi,|| Masaichiro Mizumaki,⊥ Naoki Ishimatsu,# Nozomu Hiraoka,▽ Masahiko Tsujimoto,○ Matthew G. Tucker,◆ J. Paul Attfield,‡ and Yuichi Shimakawa†

Institute for Chemical Research, Kyoto University, Uji, Kyoto 611-0011, Japan, Centre for Science at Extreme Conditions and School of Chemistry, University of Edinburgh, Mayfield Road, Edinburgh EH9 3JZ, United Kingdom, Exploratory Nanomaterials Laboratory and International Center for Materials Nanoarchitectonics (MANA), National Institute for Materials Science, Tsukuba, Ibaraki 305-0044, Japan, Japan Synchrotron Radiation Research Institute, 1-1-1 Kouto, Sayo-cho, Sayo-gun, Hyogo 679-5198, Japan, Graduate School of Science, Hiroshima University, 1-3-1 Kagamiyama, Higashi-Hiroshima 739-8526, Japan, National Synchrotron Radiation Research Center (NSRRC), 101 Hshin-Ann Road, Taiwan 30076, Republic of China, Institute for Integrated Cell-Material Sciences, Kyoto University, Yoshida-Ushinomiyacho, Kyoto 606-8501, Japan, and ISIS Facility, Rutherford Appleton Laboratory, Chilton, Didcot OX11 0QX, United Kingdom

Received April 9, 2010; E-mail: oka@issp.u-tokyo.ac.jp; masaki@scl.kyoto-u.ac.jp

Abstract: The structural and electronic properties of $BiCoO_3$ under high pressure have been investigated. Synchrotron X-ray and neutron powder diffraction studies show that the structure changes from a polar $PbTiO_3$ type to a centrosymmetric $GdFeO_3$ type above 3 GPa with a large volume decrease of 13% at room temperature revealing a spin-state change. The first-order transition is accompanied by a drop of electrical resistivity. Structural results show that Co^{3+} is present in the low spin state at high pressures, but X-ray emission spectra suggest that the intermediate spin state is present. The pressure−temperature phase diagram of $BiCoO_3$ has been constructed enabling the transition temperature at ambient pressure to be estimated as 800−900 K.

Introduction

Ferroelectric compounds generally transform to paraelectric phases at a Curie transition temperature (T_C). For example, $PbTiO_3$ changes from a polar tetragonal structure (space group $P4mm$, lattice parameter ratio $c/a = 1.064$) with a spontaneous polarization, P_S, of 59 $\mu C/cm^2$ (calculated with a point charge model) to the centrosymmetric cubic perovskite structure (space group $Pm\bar{3}m$) at $T_C = 763$ K.[1] High-pressure (HP) synchrotron X-ray powder diffraction and Raman-scattering studies found a sequence of phase transitions from tetragonal to monoclinic to another monoclinic and to rhombohedral phases with increasing pressure.[2,3] The large spontaneous polarization and the high T_C of $PbTiO_3$ result from the stereochemical $6s^2$ lone pair of Pb^{2+} and the covalent Pb−O bonds. Bi-containing perovskites may also be expected to have distorted polar structures since Bi^{3+} is similar to Pb^{2+}.

The perovskite $BiCoO_3$ was recently synthesized at high pressure[4] and is notable as a parent compound for lead-free piezoceramics.[5,6] It is isostructural with $PbTiO_3$, but the polar structural distortion is more pronounced, with a large displacement of the Co^{3+} ion from the center of the octahedron leading to a pyramidal rather than octahedral coordination. This large distortion leads to a high c/a ratio of 1.267 and a calculated P_S of 120 $\mu C/cm^2$. According to an empirical relation between T_C and the spontaneous polarization P_S (in $\mu C/cm^2$), $T_C = (0.303 \pm 0.018)P_S^2$ (eq 1),[1] the T_C of $BiCoO_3$ is expected to be ∼4500 K. However, the transition of $BiCoO_3$ to a paraelectric phase has not been observed under atmospheric pressure (AP) because of sample decomposition at 733 K. Investigation of the structural transition under high pressure conditions is therefore of particular interest to enable the T_C of $BiCoO_3$ at ambient pressure to be estimated by extrapolating the phase boundary in the P−T phase diagram.

Another interest in $BiCoO_3$ is the spin state of the Co^{3+} ion. $BiCoO_3$ exhibits C-type antiferromagnetic ordering below the

† Institute for Chemical Research, Kyoto University.
‡ Centre for Science at Extreme Conditions and School of Chemistry, University of Edinburgh.
§ Exploratory Nanomaterials Laboratory, National Institute for Materials Science.
|| International Center for Materials Nanoarchitectonics (MANA), National Institute for Materials Science.
⊥ Japan Synchrotron Radiation Research Institute.
Graduate School of Science, Hiroshima University.
▽ National Synchrotron Radiation Research Center.
○ Institute for Integrated Cell-Material Sciences, Kyoto University.
◆ ISIS Facility, Rutherford Appleton Laboratory.

(1) Abrahams, S. C.; Kurtz, S. K.; Jamieson, P. B. *Phys. Rev.* **1968**, *172*, 551.
(2) Ahart, M.; Somayazulu, M.; Cohen, R. E.; Ganesh, P.; Dera, P.; Mao, H. K.; Hemley, R. J.; Ren, Y.; Liermann, P.; Wu, Z. G. *Nature* **2008**, *451*, 545.
(3) Janolin, P.-E; Bouvier, P; Kreisel, J; Thomas, P. A.; Kornev, I. A.; Bellaiche, L; Crichton, W.; Hanfland, M.; Dkhil, B. *Phys. Rev. Lett.* **2008**, *101*, 237601.
(4) Belik, A. A.; Iikubo, S.; Kodama, K.; Igawa, N.; Shamoto, S.; Niitaka, S.; Azuma, M.; Shimakawa, Y.; Takano, M.; Izumi, F.; Takayama-Muromachi, E. *Chem. Mater.* **2006**, *18*, 798.
(5) Azuma, M.; Niitaka, S.; Hayashi, N.; Oka, K.; Takano, M.; Funakubo, H.; Shimakawa, Y. *Jpn. J. Appl. Phys.* **2008**, *47*, 7579.
(6) Nakamura, Y.; Kawai, M.; Azuma, M.; Shimakawa, Y. *Jpn. J. Appl. Phys.* **2010**, *49*, 051501.

 10.1021/ja102987d

Néel temperature (T_N) of 420 K at ambient pressure.[4] The ordered magnetic moment at 5 K is 3.24 μ_B, indicating that Co^{3+} is in the high-spin (HS) $t_{2g}^4e_g^2$ state. This is in contrast to $LaCoO_3$ where Co^{3+} is in the low-spin (LS) state at the lowest temperature and changes to intermediate spin (IS) and HS states at higher temperatures.[7,8] Recently, we proposed a scenario where the HS d^6 electronic configuration of Co^{3+} amplifies the structural distortion of $BiCoO_3$.[9] Assuming five electrons out of six are distributed to each of the five d orbitals, the tetragonal distortion is induced so that the last one goes into the nondegenerate d_{xy} orbital located at the lowest energy. The d_{xy} orbital is further from the short apical oxide anion, so the energy of the d_{xy} orbital is lowered more than the degenerate d_{yz} and d_{zx} ones. Hence, the pyramidal coordination is stabilized in the HS d^6 system to lift the orbital degeneracy. This model is analogous to the off-center vanadyl distortion commonly observed in V^{4+} (d^1) oxides and oxo complexes, although it is less frequently observed in HS Co^{3+} compounds and appears to be driven cooperatively by the Bi^{3+} distortion in $BiCoO_3$. In this context, a change to either the IS or LS states is expected in the paraelectric phase. Recent theoretical calculations support this intuitive expectation. Ravindran predicts LS Co^{3+} in the paraelectric cubic phase which is denser than the tetragonal ambient pressure (AP) phase by 5%.[10] Ming proposed a HS−LS transition driven by a volume compression of 4.87% even without a paraelectric transition.[11]

To clarify the structural and electronic changes under high pressure, we have carried out synchrotron X-ray and neutron powder diffraction (SXRD and NPD) measurements. The change of the electronic state during the structural transition was studied by using a resistivity measurement, and the spin states of Co^{3+} have been investigated by X-ray emission spectroscopy (XES).

Experimental Section

A polycrystalline $BiCoO_3$ sample for the high-pressure SXRD studies was prepared with a belt-type apparatus from stoichiometric mixtures of Bi_2O_3, Co_3O_4, and $KClO_3$ sealed in a Au capsule at 6 GPa and 1200 °C for 1 h.[4] The obtained $BiCoO_3$ was carefully crushed into a fine powder and put in a symmetric-type diamond anvil cell (DAC) with a pressure medium (methanol/ethanol/water = 16:3:1) to provide hydrostatic conditions. The pressure was determined using the ruby fluorescence method.[12] The powder diffraction data obtained using monochromated X-rays ($\lambda = 0.32698$ Å) were recorded on a flat imaging plate at the beamline BL04B2 of SPring-8 with a sample-to-detector length of 488.814 mm. Details of the SXRD technique, including the data treatments, are described elsewhere.[13]

The $BiCoO_3$ sample for other measurements was prepared with a cubic anvil-type high-pressure apparatus at 6 GPa and 1000 °C for 0.5 h. Energy-dispersive SXRD experiments were conducted for phase identification at HP and high-temperature (HT) conditions with a cubic anvil-type HP apparatus SMAP-2 installed at BL14B1 of SPring-8. Time-of-flight (TOF) NPD data at HP-HT and low-temperature (LT) conditions were recorded with the instrument PEARL/HiPr at the ISIS facility, U.K. About 90 mm^3 of the sample was loaded into a Paris−Edinburgh cell[14] with 4:1 methanol−ethanol as a pressure medium and a small pellet of lead as the pressure calibrant. Cooling and heating of the sample at pressure were achieved using the newly commissioned variable-temperature insert.[15] Rietveld profile refinements of the structural models were performed with the GSAS software.[16]

An electrical resistance measurement at HP−HT conditions was performed with a cubic anvil-type high-pressure apparatus by a four-point probe method. Gold electrodes were deposited on both faces of a disk-shaped sample (φ4 mm × 1.7 mm). The pressure medium was pyrophyllite.

The XES measurements were performed at the Taiwan IXS Beamline BL12XU at SPring-8 in Japan. The sample was put in a symmetric type DAC with Daphne oil 7373 as a pressure medium. The pressure was determined using the ruby fluorescence method. A total energy resolution was set to 1.1 eV. The incident beam was monochromatized by a Si 111 double-crystal monochromator and was then focused into a spot of 22 (horizontal) × 50 (vertical) μm^2 at the sample position with a Kirkpatrick−Baez (KB) mirror. The emitted X-rays were analyzed using a Ge 444 spherically bent analyzer of 1 m radius. The energy spectra were measured by rotating the analyzer in the Bragg mode, synchronized with the detector motion so as to maintain the Roland condition. The XES spectra were finally normalized to the spectral area.

Results and Discussion

The SXRD patterns of $BiCoO_3$ at various pressures below 6 GPa are shown in Figure 1a. A structural transition from the tetragonal $PbTiO_3$-type (space group *P*4*mm*) to the orthorhombic $GdFeO_3$-type (space group *Pbnm*) was clearly observed between 2.4 and 4.4 GPa in compression and below 1.8 GPa in decompression. No further structural transition was observed up to 10 GPa. The unit cell ($a = 5.2714$ Å, $b = 5.3390$ Å, and $c = 7.5049$ Å at 8.3 GPa) of the high-pressure phase is a $\sqrt{2} \times \sqrt{2} \times 2$ superstructure of the cubic perovskite ($Pm\bar{3}m$) cell. The transition pressure is about 1/3 of that of $PbTiO_3$, which shows the first transition to a monoclinic phase at 10 GPa.[2] Figure 1b shows the pressure dependence of the cell volume per formula unit of the AP and HP phases. A large volume drop of 13% was observed at the transition pressure. The pressure-induced phase transition of $BiCoO_3$ is first order, unlike that of $PbTiO_3$, which shows a second-order phase transition.[2] The unit cell volumes (V) of the two phases as a function of pressure (P) were fitted with the second order Birch−Murnaghan equation of state, $P = (3/2)K_0[(V_0/V)^{7/3} - (V_0/V)^{5/3}]$, where K_0 is the bulk modulus and V_0 is the volume at ambient pressure.[17] Fitting gives $K_0 = 74(3)$ GPa and $V_0 = 65.73(5)$ $Å^3$ for the AP phase and $K_0 = 104(3)$ GPa and $V_0 = 56.70(5)$ $Å^3$ for the HP phase, respectively. This confirms that the HP phase is denser and less compressible than the AP structure.

The limited number of particles in the small sample space of DAC resulted in some spotlike reflections influencing the intensity of the Debye rings. This incomplete powder averaging prevented accurate atomic coordinates from being obtained from the SXRD data. Hence, NPD studies were carried out at HP and HT conditions to determine the atomic positions in the HP phase and also to construct the P−T phase diagram. Figure 2

(7) Yamaguchi, S.; Okimoto, Y.; Taniguchi, H.; Tokura, Y. *Phys. Rev. B* **1996**, *53*, 2926.
(8) Yamaguchi, S.; Okimoto, Y.; Tokura, Y. *Phys. Rev. B* **1997**, *55*, 8666.
(9) Oka, K.; Yamada, I.; Azuma, M.; Takeshita, S.; Satoh, K. H.; Koda, A.; Kadono, R.; Takano, M.; Shimakawa, Y. *Inorg. Chem.* **2008**, *47*, 7355.
(10) Ravindran, P.; Vidya, R.; Eriksson, O.; Fjellvag, H. *Adv. Mater.* **2008**, *20*, 1353.
(11) Ming, X.; Meng, X.; Hu, F.; Wang, C. Z.; Huang, Z. F.; Fan, H. G.; Chen, G. *J. Phys.: Condens. Matter* **2009**, *21*, 295902.
(12) Mao, H. K.; Xu, J.; Bell, P. M. *J. Geophys res.* **1986**, *91*, 4673.
(13) Yusa, H.; Sata, N.; Ohishi, Y. *Am. Mineral.* **2007**, *92*, 648.
(14) Besson, J. M.; Nelmes, R. J.; Hamel, G.; Loveday, J. S.; Weill, G.; Hull, S. *Phys. B (Amsterdam, Netherlands)* **1992**, *180*, 907.
(15) Marshall, W. G.; Francis, D. J.; Barry, C. J.; Tucker, M. G.; Pulham, C. R.; Kouzmenko, G; Kirichek, O.; *Rev. Sci. Instrum.*, in press.
(16) Larson, A. C.; Von Dreele, R. B. *General Structural Analysis System (GSAS)*; Los Alamos National Laboratory Report; Los Almos National Laboratory: Los Alamos, NM, 2000; pp 86−748.
(17) Birch, F. *J. Geophys. Res.* **1952**, *57*, 227.

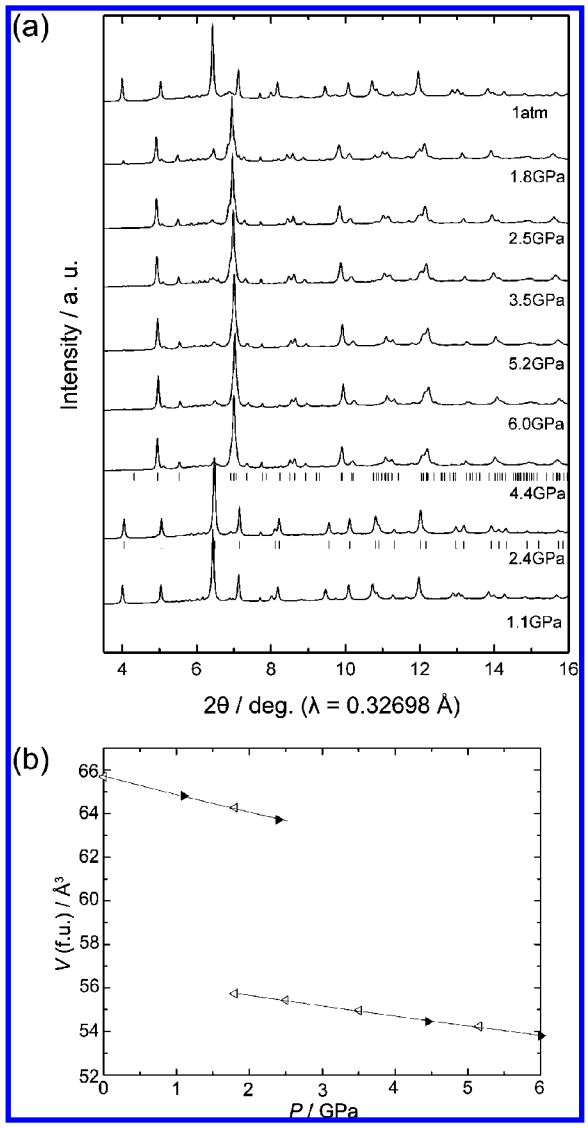

Figure 1. (a) SXRD patterns of $BiCoO_3$ collected at various pressures during compression (lower patterns) and decompression (upper patterns). The wavelength was $\lambda = 0.32698$ Å. Tick marks at the bottom of the patterns at 2.4 and 4.4 GPa denote Bragg reflections of *P4mm* and *Pbnm* perovskites, respectively. (b) Pressure dependence of the cell volume per formula unit. Solid and open symbols represent the data under compression and decompression, respectively. The solid curves represent the fit of the Birch−Murnaghan equation of state as discussed in the text.

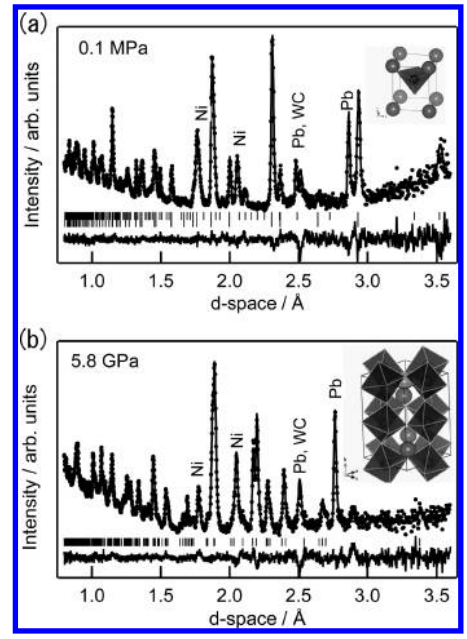

Figure 2. Time-of-flight neutron powder diffraction data for $BiCoO_3$ at 300 K. (a) Rietveld fits of the tetragonal structure to ambient pressure (0.1 MPa) data ($a = 3.7310(2)$ Å, $c = 4.7247(5)$ Å), fitting residuals; $\chi^2 = 1.69$, $R_{WP} = 2.48\%$. (b) Rietveld fits of the orthorhombic structure to high-pressure (5.8 GPa) data ($a = 5.2963(7)$ Å, $b = 5.3936$ (1) Å, $c = 7.5469(11)$ Å), fitting residuals; $\chi^2 = 1.82$, $R_{WP} = 2.02\%$. Observed (points), calculated (solid line), and difference profiles are shown together with Bragg markers for $BiCoO_3$. The upper and lower tick marks for AP phase represent the crystal diffraction and magnetic diffraction, respectively. (The contributions of Pb as a pressure marker and Ni and WC from the apparatus were also fitted.) Insets in (a) and (b) show the AP and HP crystal structures, respectively.

Table 1. Crystallographic Parameters from 300 K NPD Refinements of $BiCoO_3$ at 0.1 MPa and 5.8 GPa

atom	site	*x*	*y*	*z*	U_{iso} (Å²)
			0.1 MPa[a]		
Bi	1a	0	0	0	0.0015(7)[c]
Co	1b	0.5	0.5	0.5699(22)	0.0015(7)[c]
O1	1b	0.5	0.5	0.2001(13)	0.0114(10)
O2	2c	0.5	0	0.7266(9)	0.0042(8)
			5.8 GPa[b]		
Bi	4c	0.9960(14)	0.0417(8)	0.25	0.0004(6)[d]
Co	4a	0	0.5	0	0.0004(6)[d]
O1	4c	0.0777(15)	0.4844(12)	0.25	0.0038(13)
O2	8d	0.7067(10)	0.2906(9)	0.0404(7)	0.0054(10)

[a] Space group *P4mm*, $a = 3.7310(2)$ Å, $c = 4.7247(5)$ Å, m_z (Co) = 3.08(9) μ_B, $Z = 1$, $\chi^2 = 1.69$, $R_{WP} = 2.48\%$. [b] Space group *Pbnm*, $a = 5.2963(7)$ Å, $b = 5.3936(6)$ Å, $c = 7.5469(11)$ Å, $Z = 4$, $\chi^2 = 1.82$, $R_{WP} = 2.02\%$. [c] The isotropic thermal parameters of Bi and Co are constrained to be equal. [d] The isotropic thermal parameters of Bi and Co are constrained to be equal.

shows the NPD patterns and the crystal structures at AP and at 5.8 GPa. The refined structural parameters and the selected bond distances and angles for AP and HP phases are summarized in Tables 1 and 2. The oxygen coordinations of Co^{3+} ions in the AP and HP phases are illustrated in Figure 3.

The pyramidal polar coordination of Co^{3+} in the AP phase changes to an almost isotropic octahedral coordination in the HP phase. The large volume change at the structural transition is mainly owing to the shrinkage of the *c* axis. The longest Co−O bond length in the AP phase, 2.977 Å, is 55% longer than that in the HP phase, while the shortest one, 1.748 Å, is only 10% shorter than that in the HP phase. These results indicate that the change from 5-fold to 6-fold coordination is the origin of the shrinkage of the *c* axis, which leads to the large volume change. The splitting of d orbitals into b_{2g} (d_{xy}), doubly degenerate e_g (d_{xz} and d_{yz}), a_{1g} (d_{z^2}), and b_{1g} ($d_{x^2-y^2}$) levels in the pyramidal coordination changes to triply degenerate t_{2g} (d_{xy}, d_{xz}, d_{yz}) and doubly degenerate e_g (d_{z^2} and $d_{x^2-y^2}$) in the octahedral cubic coordination. Since the d-level splitting in the pyramidal coordination in the AP phase is stabilized by the HS electronic configuration of Co^{3+}, the LS or IS state is expected for the HP phase with octahedral coordination. The ionic radius of Co^{3+} in the HP phase, estimated by subtracting the oxide radius of 1.40 Å from the average Co−O bond length, is 0.54 Å. This is very close to the value of 0.545 Å for the LS Co^{3+} ion in octahedral coordination.[18] A reliable ionic radius for IS Co^{3+} is not available, but an estimate from the average of HS

(18) Shannon, R. D. *Acta Crystallogr., Sect. A* **1976**, *32*, 751.

Table 2. Selected Bond Distances (Å) and Angles (deg) for $BiCoO_3$ at 0.1 MPa and 5.8 GPa from the Refinements in Table 1

0.1 MPa		5.8 GPa			
Bi−O1 (×4)	2.802(3)	Bi−O1	2.423(8)	Co−O1 (×2)	1.933(1)
Bi−O2 (×4)	2.268(3)	Bi−O1	2.278(8)	Co−O2 (×2)	1.938(5)
Bi−O2 (×4)	3.909(4)	Bi−O1	3.056(8)	Co−O2 (×2)	1.942(5)
Bi−O (avg)	2.993	Bi−O1	3.041(8)	Co−O (avg, 6-fold)	1.938
Co−O1	1.748(13)	Bi−O2 (×2)	2.580(8)	Co1−O1−Co1	154.8(3)
Co−O1	2.977(13)	Bi−O2 (×2)	2.345(8)	Co1−O2−Co1	153.9(3)
Co−O2 (×4)	2.008(4)	Bi−O2 (×2)	2.617(8)		
Co−O (avg, 5-fold)	1.956	Bi−O2 (×2)	3.239(8)		
Co1−O2−Co1	136.6(3)	Bi−O (avg)	2.697		

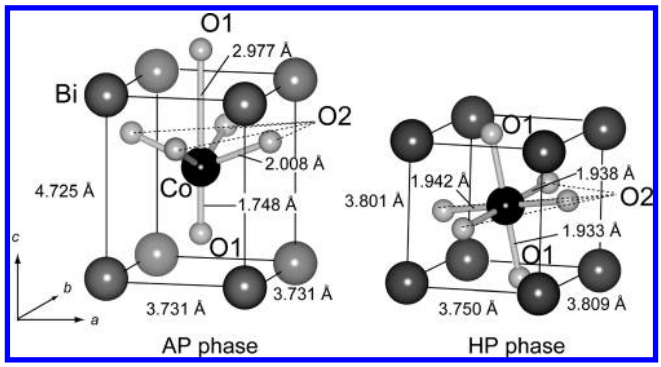

Figure 3. Illustrations of the coordination environments of Co^{3+} in the AP and HP phases of $BiCoO_3$.

and LS radii is 0.58 Å. The distribution of the bond lengths in the HP phase is less than 0.5%, indicating the absence of Jahn−Teller distortion, which is expected for the IS Co^{3+}.[8,19,20] These results suggest that a HS to LS state change accompanies the pressure-induced ferroelectric to paraelectric structural transition as theoretically predicted.[10]

Figure 4a shows the P−T phase diagram for $BiCoO_3$ determined by our SXRD and NPD studies. The data points collected on pressurizing or on heating are plotted. $BiCoO_3$ keeps the tetragonal structure up to the decomposition temperature of 733 K at ambient pressure. However, a temperature-induced transition is observed by heating at a moderate pressure, and the temperature dependence of the unit cell at around 2.4 GPa is shown in Figure 4b. $BiCoO_3$ undergoes a first-order transition from the tetragonal phase at AP−LT conditions to the orthorhombic phase at HP−HT through a two-phase region. The average volumes decreases on heating across a wide temperature range of 200−350 K, and the phase boundary is shaded in the phase diagram. The structural transition temperature at AP was estimated to be 800−900 K by extrapolating the boundary to 0.1 MPa. This value is only about 1/5 of the 4500 K estimated from eq 1.[1] $BiFeO_3$ is also known to possess a large spontaneous polarization of 90−100 $\mu C/cm^2$,[21] however, the T_C of $BiFeO_3$ is 1100 K,[22] which is 1/3 of the value estimated from eq 1. Hence this equation is not reliable for BiMO_3-type ferroelectrics with magnetic ions in the *B*-sites. It is also interesting to point out the similarities of the high pressure phases of $BiMO_3$. $BiScO_3$,[23] $BiCrO_3$,[23] $BiFeO_3$,[24,25] $BiMnO_3$,[23] and $BiNiO_3$[26] are all known to change to $GdFeO_3$-type structures

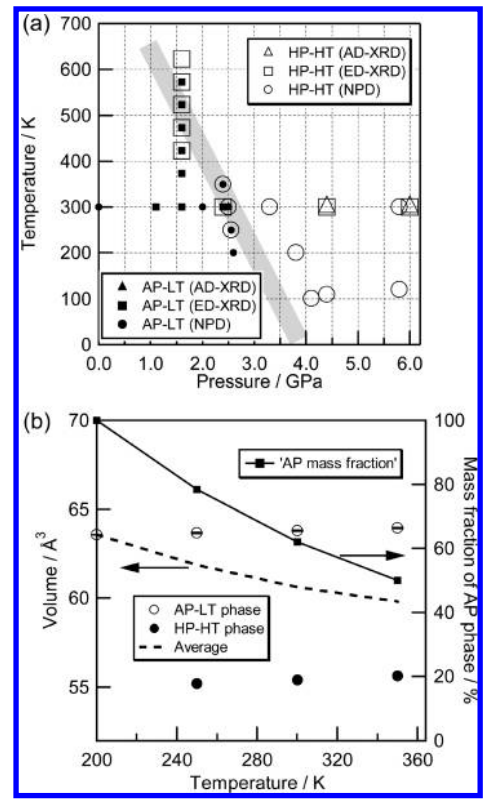

Figure 4. (a) Pressure−temperature diagram for $BiCoO_3$ determined by the angle-dispersive (AD) XRD (triangles), energy-dispersive (ED) XRD (squares), and NPD (circles) experiments. The filled and open symbols represent the AP-LT and HP-HT phases, respectively. The shaded region indicates the phase boundary. (b) Temperature dependence of the cell volume per formula unit and the mass fraction of AP phase at 2.4 GPa.

under HP conditions as does $BiCoO_3$ despite the variety of structural distortions at AP.

The structural transition in $BiCoO_3$ is coupled to a change of electronic properties. Figure 5a shows the pressure dependence of the electrical resistivity for $BiCoO_3$. The resistivity decreases by 3 orders of magnitude at the structural transition pressure of 2−3 GPa. The resistivity of the HP phase measured at 6 GPa shown in Figure 5b, however, decreases with increasing temperature, indicating that this phase is semiconducting. The

(19) Korotin, M. A.; Ezhov, S. Y.; Solovyev, I. V.; Anisimov, V. I.; Khomskii, D. I.; Sawatzky, G. A. *Phys. Rev. B* **1996**, *54*, 5309.
(20) Mizokawa, T.; Khomskii, D. I.; Sawatzky, G. A. *Phys. Rev. B* **1999**, *60*, 7309.
(21) Neaton, J. B.; Ederer, C.; Waghmare, U. V.; Spaldin, N. A.; Rabe, K. M. *Phys. Rev. B* **2005**, *71*, 014113.
(22) Teague, J. R.; Gerson, R.; James, W. J. *Solid State Commun.* **1970**, *8*, 1073.
(23) Belik, A. A.; Yusa, H.; Hirao, N.; Ohishi, Y.; Takayama-Muromachi, E. *Inorg. Chem.* **2009**, *48*, 1000.
(24) Belik, A. A.; Yusa, H.; Hirao, N.; Ohishi, Y.; Takayama-Muromachi, E. *Chem. Mater.* **2009**, *21*, 3400.
(25) Haumont, R.; Bouvier, P.; Pashkin, A.; Rabia, K.; Frank, S.; Dkhil, B.; Crichton, W. A.; Kuntscher, C. A.; Kreisel, J. *Phys. Rev. B* **2009**, *79*, 184110.
(26) Azuma, M.; Carlsson, S.; Rodgers, J.; Tucker, M. G.; Tsujimoto, M.; Ishiwata, S.; Isoda, S.; Shimakawa, Y.; Takano, M.; Attfield, J. P. *J. Am. Chem. Soc.* **2007**, *129*, 14433.

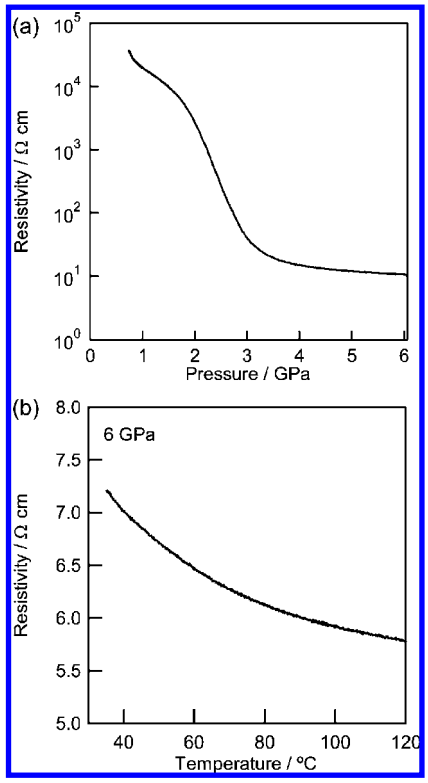

Figure 5. (a) Pressure dependence of the resistivity at 300 K and (b) temperature dependence of the resistivity at 6 GPa of $BiCoO_3$.

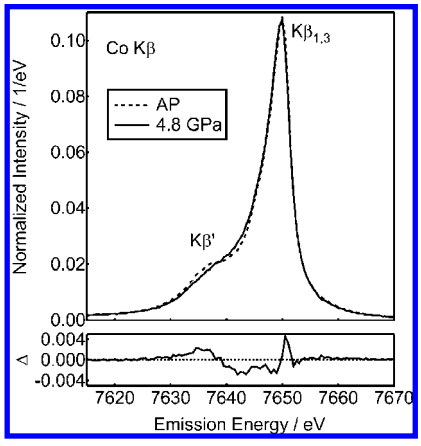

Figure 6. Co $K\beta$ X-ray emission spectra (XES) of the AP-LT and HP-HT phases of $BiCoO_3$. The spectra at 0.1 MPa (broken line) and at 4.8 GPa (solid line) are shown. Both spectra were normalized to have integrated intensity = 1.0 in the energy range of 7615−7670 eV. Δ is the difference of normalized intensity, $I_{AP} - I_{HP}$.

metallicity predicted for the cubic HP phase by Ravindran[10] and the semimetallicity for the tetragonal phase with reduced *c*/*a* by Ming[11] were not observed. This disagreement is probably because of the heavily buckled Co−O−Co bonds in the $GdFeO_3$-type structure of the HP phase. A band calculation based on the $GdFeO_3$-type orthorhombic structure determined in this study will be useful to resolve these issues.

As the structural analysis suggested the presence of a pressure-induced spin state change, the spin state of Co^{3+} was further investigated by Co $K\beta$ XES measurements. Figure 6 shows the XES spectra at room temperature and at 0.1 MPa and at 4.8 GPa along with their difference. The Co $K\beta_{1,3}$ emission line with a low energy satellite $K\beta'$ was clearly observed at 0.1 MPa. However, the $K\beta'$ is less pronounced in the spectrum at 4.8 GPa which indicates a decrease of the magnetic moment, and this is also reported for $LaCoO_3$ across the temperature and pressure induced HS to LS change.[27,28] Although the XES spectra are made up by contributions from numerous terms, it is known that the change in the spin number, ΔS, is proportional to the integrated absolute value of the difference (IAD) spectra,[27−30] IAD = 0.049 for $\Delta S = 1$, 0.084 for $\Delta S = 3/2$ and = 0.12 for $\Delta S = 2$. We calculated the IAD value according to refs 27 and 28 using $\Sigma|I_{AP} - I_{HP}|$ in the energy range of 7615−7670 eV, where I_{AP} and I_{HP} are the normalized intensities of XES spectra for the AP and HP phases, respectively, and obtained an IAD value = 0.041 for $BiCoO_3$. This suggests $\Delta S = 1$, i.e., an IS state for the Co^{3+} in the HP phase. This result is in contrast to the result of our structural analysis suggesting the LS state for the HP phase. The reason for this discrepancy is not clear at this stage. Several possibilities such as fluctuating orbital ordering without Jahn−Teller distortion or underestimation of ΔS because of the influence of the drastic local structural distortion on the XES spectra can be proposed. If Co^{3+} is in the IS state with $S = 1$, then the HP phase should be magnetic and antiferromagnetic ordering might be expected for the HP phase, analogous to the G-type spin order observed in the insulating phase of $BiNiO_3$.[26] Our HP neutron data do not extend to sufficiently long d-spacings to allow magnetic order to be observed so this possibility is not confirmed or excluded. The magnetism and spin state of the HP phase of $BiCoO_3$ will require further studies such as by NMR.

Finally, we compare the spin-state change in $BiCoO_3$ to that observed in $LaCoO_3$. The spin-state change in $LaCoO_3$ results from the competition between the crystal field energy and the intra-atomic (Hund) exchange energy.[7,19,31,32] The LS Co^{3+} state of $LaCoO_3$ achieved under HP or LT conditions is attributed to the increase of the crystal field energy owing to the thermal contraction of the Co−O bonds.[7,28,33−35] In contrast, $BiCoO_3$ keeps the HS Co^{3+} state down to the lowest temperatures. The present study revealed that Co^{3+} in the paraelectric phase above 3 GPa at 300 K is in either the IS or the LS state. For both $LaCoO_3$ and $BiCoO_3$, application of pressure stabilizes phases with reduced magnetic moments.

Conclusions

We have investigated the structural transition of $BiCoO_3$ under high pressure by powder synchrotron X-ray and neutron diffraction studies. $BiCoO_3$ changes from a $PbTiO_3$-type tetragonal structure to a $GdFeO_3$-type orthorhombic structure above 3 GPa with a large volume change of 13%. The same structural change takes place when $BiCoO_3$ is heated at moderate

(27) Vanko, G.; Rueff, J. P.; Mattila, A.; Nemeth, Z.; Shukla, A. *Phys. Rev. B* **2006**, *73*, 024424.
(28) Lengsdorf, R.; Rueff, J. P.; Vanko, G.; Lorenz, T.; Tjeng, L. H.; Abd-Elmeguid, M. M. *Phys. Rev. B* **2007**, *75*, 180401.
(29) Vanko, G.; Neisius, T.; Molnar, G.; Renz, F.; Karpati, S.; Shukla, A.; de Groot, F. M. F. *J. Phys. Chem. B* **2006**, *110*, 11647.
(30) Rueff, J. P.; Shukla, A.; Kaprolat, A.; Krisch, M.; Lorenzen, M.; Sette, F.; Verbeni, R. *Phys. Rev. B* **2001**, *63*, 132409.
(31) Tokura, Y.; Okimoto, Y.; Yamaguchi, S.; Taniguchi, H.; Kimura, T.; Takagi, H. *Phys. Rev. B* **1998**, *58*, 1699.
(32) Senaris-Rodriguez, M. A.; Goodenough, J. B. *J. Solid State Chem.* **1995**, *116*, 224.
(33) Heikes, R. R.; Mazelsky, R.; Miller, R. C. *Physica* **1964**, *30*, 1600.
(34) Abbate, M.; Fuggle, J. C.; Fujimori, A.; Tjeng, L. H.; Chen, C. T.; Potze, R.; Sawatzky, G. A.; Eisaki, H.; Uchida, S. *Phys. Rev. B* **1993**, *47*, 16124.
(35) Barman, S. R.; Sarma, D. D. *Phys. Rev. B* **1994**, *49*, 13979.

pressures. The structural data show that Co^{3+} is present in the low spin state at high pressures, but Co $K\beta$ XES spectra suggest that the intermediate spin state is present at the transition. The ferroelectric T_C of $BiCoO_3$ was estimated to be 800−900 K by extrapolating the phase boundary in the P−T phase diagram to ambient pressure.

Acknowledgment. We express our thanks to Prof. Tamio Oguchi for fruitful discussions. We are also grateful to Y. Ohishi and N. Hirao for technical help during X-ray measurement at SPring-8 and to Mr. M. Senn (CSEC and School of Chemistry, The University of Edinburgh, U.K.) for help with the neutron powder diffraction measurements. This work was partially supported by Grants-in-Aid from the Ministry of Education, Culture, Sports, Science and Technology, Japan, for Scientific Research (Nos. 19GS0207, 19340098, and 19052008) and the Elements Science and Technology Project and for a Joint Project of the Chemical Synthesis Core Research institutions. K.O. was supported by Research Fellow of the Japan Society for the promotion of science. H.Y. and A.A.B. acknowledge support from NIMS Competitive Research Fund. The AD SXRD experiments were conducted at BL04B2 of SPring-8 with the approval of JASRI (Proposal Nos. 2006B1134 and 2007B1192). The ED SXRD experiments were performed at JAEA beamline BL14B1 SPring-8 under Proposal No. 2008A-E6. The XES experiments were performed at Taiwan beamline BL12XU SPring-8 under Proposal No. 2009A4253 (JASRI)/2009-2-036-1 (NSRRC). The neutron diffraction experiment was done under the Strategic Japanese-UK Cooperative Program funded by JST and EPSRC. Support was also provided by EPSRC and the Leverhulme Trust, U.K.

JA102987D